Development of the dynamic and static joint leveling control system for vehicle-mounted platform in mountain tea plantations

Haijun Zhu, Hongling Jin*, Shujie Wang, Mingyang Qin, Yu Chen, Shuo Zhang

(*School of Mechanical and Electronic Engineering, Northwest A & F University, Yangling 712100, Shaanxi, China*)

Abstract: Tea is one of the three major beverages in the world, and China, as the world's largest tea producer and consumer, faces challenges in addressing the poor stability and low efficiency of self-propelled tea canopy working machines when operating in mountainous tea plantations. The static leveling systems alone are insufficient to solve this issue. This paper presents a dynamic and static joint leveling control system based on Proportional-Integral-Derivative (PID), utilizing a self-developed vehicle-mounted omnidirectional leveling platform. The analysis of the platform's leveling principle and the construction of its hardware control system are discussed, then a joint control method for dynamic and static leveling is formulated. Simulation tests were conducted to determine the control parameters of the leveling system, validating the effectiveness of the control system. A prototype machine was built to test both its leveling performance and field capabilities. Results demonstrate that on a 15.0° slope, the platform can reduce inclination to less than 5.0° within 1.0 s, with an inclination error controlled at 0.1°-0.4° within 1.8-2.3 s; during field tests, mean inclination values when entering and exiting tea plantations are measured at 3.2°±1.5° and 2.5°±1.4°, respectively. The results indicate that this developed dynamic and static joint leveling control system enables rapid platform stabilization while reducing tipping risks in mountainous tea plantations.

Keywords: vehicle-mounted platform, staged PID algorithm, dynamic and static joint leveling, omnidirectional leveling, control system

DOI: 10.25165/j.ijabe.20261902.9649

Citation: Zhu H J, Jin H L, Wang S J, Qin M Y, Chen Y, Zhang S. Development of the dynamic and static joint leveling control system for vehicle-mounted platform in mountain tea plantations. Int J Agric & Biol Eng, 2026; 19(2): 128–138.

1 Introduction

Tea is one of the top three beverages worldwide and is renowned for its richness in nutrients such as tea polyphenols, catechins, amino acids, and caffeine[1]. The global tea production in 2022 amounted to 6.477 Mt, with China ranking first and contributing 3.181 Mt of tea production, as reported by the Tea Circulation Association. The tea plantations in China encompass a vast area of over 3.26×10^6 hm^2, establishing it as the largest in the world[2,3]. With more than 60% of these plantations located in hilly and mountainous regions[4], the intricate and steep terrain presents challenges for mechanized operations. Traditional handheld machines from Kawasaki, Japan like single tea pickers and double tea trimmers are predominantly used due to their adeptness at navigating these demanding landscapes. However, this approach leads to high labor intensity and difficulties ensuring work quality.

The development of a dynamic and static joint leveling control system for vehicle leveling platform is an effective approach to mitigate the tipping rate of small self-propelled tea canopy working machines and facilitate the mechanization of entire tea plantation production. The principle behind the leveling control entails sensor-based acquisition of the working platform's attitude or position information, subsequent processing by the controller to generate control signals, and actuator-driven adjustments made to maintain desired platform balance[5]. Currently, extensive researches by both domestic and international scholars focus on pivotal technologies such as leveling control systems, encompassing military, industrial, and agricultural domains. The initial application of the leveling control system was primarily observed in the military sector, specifically artillery and military radar[6-8]. The application of this technology has extended to various industries, including the industrial and agricultural sectors. In the industrial field, it finds utility in aerial work platforms, offshore work platforms, pavers, fire trucks, and other related equipment[9-12]. In the agricultural sector, chassis and work implement leveling have gained widespread application. Yang's team has enhanced the walking system of the crawler tractor to enable reversible track movement on both sides for achieving effective leveling[13,14]. Denis et al.[15] proposed an online adaptive observer and implemented the leveling of the entire machine using a 4-wheel independent hydraulic leveling mechanism. İrsel and Altinbalik[16] redesigned the existing laser-controlled leveling shovel to enhance its automation capabilities. Wang et al.[17] developed a control model for hilly mountain tractor body leveling based on tire stiffness and wheel center of mass displacement. The body leveling system of the combine harvester has been extensively investigated and enhanced by numerous scholars[18,19], leading to enhanced driving safety and operational precision of the entire vehicle. Park et al.[20,21] sequentially developed a sensor fusion-based and backstepping control-based attitude control system for the cutting device in cabbage harvesters to enhance harvesting quality. Despite the

Received date: 2025-05-30 **Accepted date:** 2026-01-21

Biographies: Haijun Zhu, PhD candidate, research interest: agricultural machinery and intelligent equipment, Email: zhuhj@nwafu.edu.cn; **Shujie Wang**, MS, research interest: agricultural machinery design and automation, Email: 1356601537@nwafu.edu.cn; **Mingyang Qin**, MS candidate, research interest: agricultural machinery design and automation, Email: 1136292963@nwafu.edu.cn; **Yu Chen**, PhD, Associate Professor, research interest: intelligent agricultural robots, Email: jdxy73@nwafu.edu.cn; **Shuo Zhang**, PhD, Associate Professor, research interest: agricultural machinery equipment and intelligent navigation, Email: zhangshuo@nwafu.edu.cn.

***Corresponding author: Hongling Jin**, PhD, Associate Professor, research interest: agricultural machinery and intelligent equipment. School of Mechanical and Electronic Engineering, Northwest A&F University, Yangling 712100, Shaanxi, China. Tel: +86-15991270635, Email: jhl@nwsuaf.edu.cn.

current advancements in agricultural machinery leveling, research primarily focuses on static platform leveling[22], with limited investigation into dynamic platform leveling control systems.

The PID algorithm, as a classical feedback control algorithm, plays a pivotal role in the agricultural machinery control system due to its relatively straightforward design and rapid system response[23-26]. Chen et al.[27] employed a PID control system to achieve the desired tool height and ensure stability in a green leaf vegetable harvester. Li et al.[28] successfully achieved anti-skid driving control for an orchard mowing robot by integrating a PID controller with a tire dynamics model. The researchers conducted comprehensive investigations on the control system of agricultural machinery for sowing and fertilizing various types of seeds, aiming to enhance the precision and quality of these processes through the implementation of PID algorithm[29-31]. The selection of parameters for the PID algorithm, however, poses a challenging task and necessitates continuous adjustment to achieve a more satisfactory control effect[32-34]. Employing simulation software to construct a control model for debugging PID control parameters can effectively reduce the cost associated with parameter tuning in order to obtain optimal values[35-37].

The objective of this paper is to design a dynamic and static joint leveling control system based on the PID algorithm, using our self-developed vehicle leveling platform as the research subject. We obtained relevant control system parameters through simulation analysis and conducted field tests to evaluate the dynamic leveling performance of the control system. This study aims to provide valuable insights for achieving complete mechanization in mountain tea plantations.

2 General design of leveling system

2.1 System structure and working principle

The structure of the leveling system is illustrated in Figure 1, which is comprised of a deflection mechanism, adaptive mechanism, and rotary mechanism. The deflection mechanism consists of the upper rotary table, lower rotary table, supporting legs, and adjusting legs. The two adjusting legs move in opposite directions to achieve a deflection angle of 0°-20°. The adaptive mechanism includes the base, telescopic mechanism, platform, etc. Lastly, the rotary mechanism comprises the toothed bearing, toothless bearing, active gear, etc. The adaptive mechanism is connected to the deflection mechanism via toothed and toothless bearings. A linear motor drives the adjusting leg, while a displacement sensor is installed adjacent to the actuator for measuring its current displacement. The lower rotary table and the base are equipped with a hall angle sensor and a slip ring. The hall angle sensor is utilized to measure the rotation angle of the deflection mechanism, while the slip ring ensures that the line remains untangled during the deflection mechanism's rotation. Additionally, an attitude sensor is installed on both the platform and the base to provide feedback on their respective pitch angles and roll angles.

The working principle of the vehicle leveling platform is as follows: when the platform is tilted, the stepper motor drives the active gear to move, and drives the deflection mechanism to rotate through the gear wheel, so that the supporting legs and the lower rotary table of the two articulated points of the line rotate to the horizontal position. Simultaneously, the coordinated movement of two linear motors within the deflection mechanism results in a deflection of the upper rotary table towards a horizontal position, thereby achieving platform levelness.

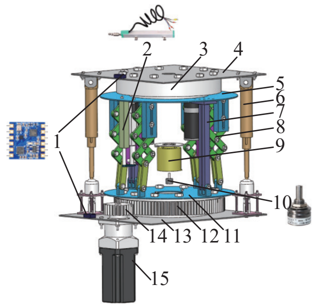

1. Attitude sensor 2. Displacement sensor 3. Toothless bearing 4. Platform 5. Upper rotary table 6. Telescopic mechanism 7. Supporting leg 8. Adjusting leg 9. Slip ring 10. Hall angle sensor 11. Lower rotary table 12. Tooth bearing 13. Base 14. Active gear 15. Stepper motor

Figure 1 Schematic structure of leveling system

2.2 Hardware design

The hardware system comprises a controller, an attitude sensor, a displacement sensor, and a hall angle sensor, among others. The electrical control principle of the control system is illustrated in Figure 2. The controller utilizes the STM32F103ZET6 microcontroller manufactured by Positive Point Atom (Guangzhou) Technology Co., Ltd., which is responsible for communication, data calculation, and sensor integration. The displacement sensor model employed is KTM produced by Taizhou Huangyan Jiemite Machinery Factory with a measurement accuracy of 0.05 mm within a range of 0-100 mm. The hall angle sensor model P3020, manufactured by Shanghai Panzhuo Automation Science and Technology Co., Ltd., offers a measurement accuracy of 0.003° within a range of 0 to 360°. Both the displacement sensor and the hall angle sensor provide analog outputs that can be directly connected to the microcontroller's I/O port for obtaining attitude information regarding the deflection mechanism in its current state. The attitude sensors used in the base and platform are IMU901 produced by Positive Point Atomics (Guangzhou) Technology Co., Ltd. These sensors utilize the USART serial port for communication with the controller, providing output of attitude angles and acceleration along three axes. The data output frequency can reach a maximum of 250 Hz, with a measurement accuracy of 0.1°, enabling acquisition of real-time attitude information for both the base and platform. The controller performs analysis and processing on data collected from hall angle sensors, displacement sensors, and attitude sensors, subsequently generating signals to control linear motor displacement and stepper motor rotation angles.

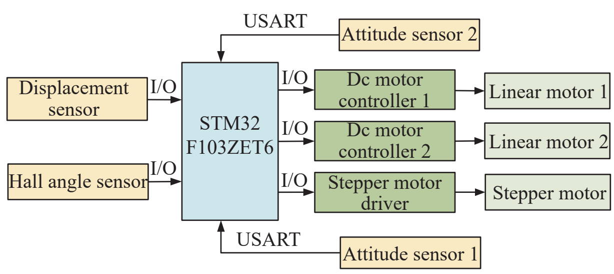

Figure 2 Electric control schematic diagram of leveling control system

The linear motor is equipped with DC motors, specifically controlled by the DC motor controller (Model: ATK-PD6010D, Positive Point Atom (Guangzhou) Technology Co., Ltd., Guangzhou, Guangdong, China). The controller regulates the pulse frequency to drive the stepper motor driver (Model: DMA860H, Wenzhou Pufeide Electromechanical Co., Ltd., Wenzhou, Zhejiang, China), enabling it to execute precise movements and coordinate motion with two linear motors. The stepper motor has a step angle of 1.8°. Both the DC motor controller and stepper motor driver are connected to the microcontroller's I/O port.

3 Dynamic and static joint leveling strategies

Due to the presence of random pits, slope rises, obstacles, and other factors in the hilly mountainous terrain, it becomes challenging for the chassis attitude sensor to obtain stable and smooth attitude information during motion. Therefore, the leveling control system needs to establish a platform inclination threshold. The process of dynamic and static joint leveling strategy is illustrated in Figure 3. When the leveling control system is activated, the controller acquires real-time platform attitude information. If the controller detects that the platform inclination exceeds the threshold, it employs dynamic leveling strategy; if it detects that the platform inclination falls below the threshold, it checks whether or not the chassis is in motion state; if it is in motion state, then the program returns to continue monitoring platform inclination; conversely, if not in motion state, the program enters static leveling strategy. It should be noted that there are currently no explicit regulations regarding residual inclination angle of the leveling platform after leveling. However, Reference [14] indicates that the overall inclination angle of a tractor with a leveling function should not exceed 5° after being leveled by the leveling mechanism. Under the premise of referring to and ensuring compliance with this limit, and based on the results of multiple tests, the dynamic leveling threshold in this paper is set at 2°. Meanwhile, considering the measurement accuracy of the sensors, the static leveling threshold is set at 0.5°.

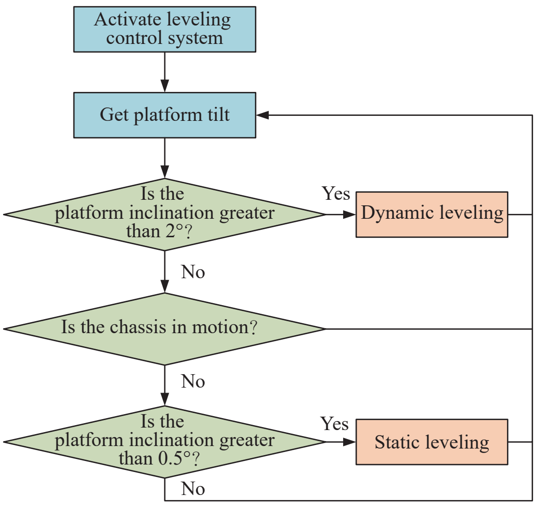

Figure 3 Leveling strategy flowchart

3.1 Dynamic control strategy

During operation, the platform attitude sensor continuously measures real-time platform attitude information. When the platform inclination exceeds a predefined threshold value, the dynamic leveling of the platform is initiated. The control strategy for dynamic leveling is illustrated in Figure 4 and comprises three main components: input part, control part, and output part. In the input part, the controller calculates the total rotation $\theta^*(t)$ and deflection $\gamma'(t)$ required for the leveling of the deflection mechanism based on chassis attitude information $\alpha(t)$ and $\beta(t)$, which are measured by the base attitude sensor. It also determines the displacement $d^*(t)$ that needs to be extended and contracted for the motorized actuator based on $\gamma'(t)$. The control deviation $e(\theta)$ and $e(d)$ are obtained by subtracting $\theta(t)$, collected by the hall angle sensor, and $d(t)$, collected by the displacement sensor, from $\theta^*(t)$ and $d^*(t)$. The input $e(\theta)$ and $e(d)$ undergo filtering in the control phase to obtain $e(t)$, followed by proportional control to determine rotational speed of the deflector mechanism $w(t)$ and the moving speed of the linear motor $v(t)$. The stepper motor control parameter f and the DC motor control parameter R_D are calculated from $w(t)$ and $v(t)$ in the output part.

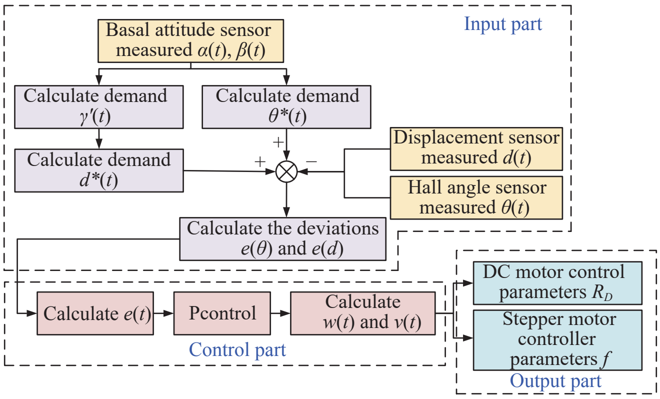

Figure 4 Dynamic leveling control strategy

3.1.1 Input part calculation

According to the dynamic leveling strategy, when there is a tilt in the base, neglecting the translational motion of the base, Figure 5 illustrates the relationship between the base coordinate system O_1-$i_1j_1k_1$ and the horizontal coordinate system O_1-$i_0j_0k_0$ at point O_1. The substrate undergoes rotation around the i_0-axis, denoted by $\alpha(t)$, and around the j_0-axis, denoted by $\beta(t)$, respectively. The inclination of the base $\gamma'(t)$ represents the angle formed between the k_1-axis and the k_0-axis, while $\theta'(t)$ denotes the angle between the positive direction of the i_0-axis and the projection of the k_1-axis onto the $i_0O_1k_0$ plane. The line AB represents the intersection between the plane $i_1O_1j_1$ and the plane $i_0O_1k_0$. The leveling principle of the leveling system is as follows: the stepper motor drives the deflection mechanism to rotate $\theta'(t)$ in order to align the supporting legs with the AB line; simultaneously, the linear motor coordinates the movement of both adjusting legs to induce the platform deflection $\gamma'(t)$ around the crossover line AB, thereby achieving platform leveling.

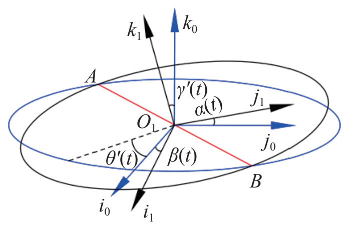

Figure 5 Relationship between the base coordinate system and the horizontal coordinate system

The leveling process of the platform can be viewed as a sequential rotation, where it first rotates $\beta(t)$ around the j_0-axis and then rotates $\alpha(t)$ around the i_0-axis[38], and the coordinate transformation matrix T is

$$\boldsymbol{T}=\begin{bmatrix}\cos\beta(t) & 0 & \sin\beta(t)\\ \sin\alpha(t)\sin\beta(t) & \cos\alpha(t) & -\sin\alpha(t)\cos\beta(t)\\ -\cos\alpha(t)\sin\beta(t) & \sin\alpha(t) & \cos\alpha(t)\cos\beta(t)\end{bmatrix} \quad (1)$$

The inclination $\gamma'(t)$ can be regarded as the angle between a unit vector $\boldsymbol{e}_1$ along the k_1-axis and a unit vector $\boldsymbol{e}_0$ along the k_0-axis. Then $\boldsymbol{e}_1$ is transformed into the coordinate system O_1-$i_0j_0k_0$, and $\boldsymbol{e}_1'$ satisfies the follows:

$$\boldsymbol{e}_1'=\boldsymbol{T}\boldsymbol{e}_1 \tag{2}$$

The substitution of Equation (1) into Equation (2) results in:

$$\boldsymbol{e}_1' = (\sin\beta(t))\boldsymbol{i}_0 - (\sin\alpha(t)\cos\beta(t))\boldsymbol{j}_0 + (\cos\alpha(t)\cos\beta(t))\boldsymbol{k}_0 \tag{3}$$

Considering the algebraic relationship, $\theta'(t)$ and $\gamma'(t)$ should respectively satisfy:

$$\theta'(t) = \frac{-\alpha(t)}{|\alpha(t)|}\arccos\frac{\sin\beta(t)}{\sqrt{\sin^2\beta(t)+\sin^2\alpha(t)\cos^2\beta(t)}} \tag{4}$$

$$\gamma'(t) = \arccos(\cos\alpha(t)\cos\beta(t)) \tag{5}$$

The value of $\theta'(t)$ is [–180°, 180°], and the value of $\gamma'(t)$ is [0, 20°]. In order to make the $\theta'(t)$ value range consistent with the sensor measurement range, the expression of $\theta^*(t)$ after the transformation is

$$\begin{cases}\theta^*(t)=360+\theta'(t), & (\beta(t)<0)\\ \theta^*(t)=\theta'(t), & (\beta(t)>0)\end{cases} \tag{6}$$

According to the leveling principle, $\gamma'(t)$ needs to be converted into the telescoping displacement $d'(t)$ of the adjusting leg. The motion diagram of the adjusting leg is shown in Figure 6. The length of connecting rod EH is denoted by l_{EH}, Q is the midpoint of the Q_1Q_2 connection, and l_{HQ} denotes the distance between points H and Q. During the leveling process, point E moves to E' while point H moves to H'. The leg's telescoping distance matches the distance of the point E, $d'(t)$ can be expressed as,

$$d'(t) = a_{HH'} + (-1)^i(a_{EH} - a_{E'H'}) \tag{7}$$

where, $(-1)^i$ indicates whether the leg is extended (i=0) or contracted (i=1); $a_{HH'}$ is the vertical distance between points H and H', mm; a_{EH} is the vertical distance between points E and H, mm; $a_{E'H'}$ is the vertical distance between points E' and H', mm.

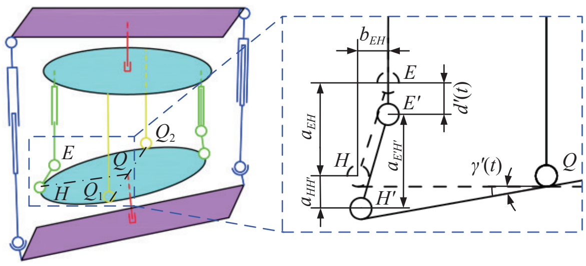

Figure 6 Leveling motion diagram

According to the details shown in Figure 6, $a_{HH'}$ and $a_{E'H'}$ can be expressed as,

$$a_{HH'} = l_{HQ}\sin\gamma'(t) \tag{8}$$

$$a_{E'H'} = \sqrt{l_{EH}^2 - \left(b_{EH} - l_{HQ}\left(1-\cos\gamma'(t)\right)\right)^2} \tag{9}$$

where, b_{EH} is the horizontal distance between points E and H, mm. According to the design parameters: a_{EH}=69.89 mm, b_{EH}=4 mm, l_{EH}=70 mm, l_{HQ}=150 mm. Substituting Equation (8) and Equation (9) into Equation (7) yields

$$d'(t) = 150\sin\gamma'(t) + (-1)^i\cdot \left(69.89 - \sqrt{-22\,500\cos^2\gamma'(t) + 43\,800\cos\gamma'(t) - 16\,416}\right) \tag{10}$$

The adjustment of the distance $d'(t)$ of point E in the supporting leg is the result of amplifying the motion speed of the linear motor by the diamond mechanism. The magnification of the diamond mechanism is 3.25. When $\gamma'(t)$ changes at 0°-20°, the extension range of the linear motor is 0-15.81 mm, and the contraction range is 0-15.76 mm. The variation curve of the linear motor's moving distance $d'(t)$ with respect to the deflection angle $\gamma'(t)$ can be obtained, then an approximate function is used for fitting. The correlation between the leg extension and contraction is illustrated in Figure 7.

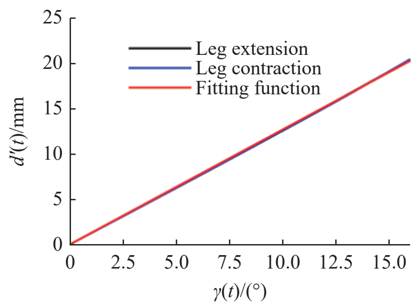

Figure 7 Variation curve of $d'(t)$ with $\gamma'(t)$ during leg extension and contraction

The relationship between the two approximately follows the direct proportional function. The least square method is employed to fit the function, and the approximation $d^*(t)$ of $d'(t)$ is

$$d^*(t) = k_d\gamma'(t) \tag{11}$$

where, the proportional constant k_d=0.79. From Figure 7, the fitting function coincides with the height of the curve obtained by the extension and contraction of the leg. However, due to inherent fitting error in the function, the telescoping amount derived from the fitting curve differs from the ideal value. The curve in Figure 8 illustrates the variation of leg stretching error with inclination $\gamma'(t)$. As depicted in Figure 8, the absolute error amplitude during leg contraction is 0.11 mm, slightly exceeding the amplitude of 0.07 mm observed during leg extension. The two extreme values of absolute error, –0.11 mm and +0.11 mm, occur at $\gamma'(t)$ values of 10.8° and 20° respectively during the leg contraction, while the corresponding platform's deflection angle errors are both measured at a mere 0.14°, significantly below the leveling threshold. Hence, employing a fitting function for dynamic leveling proves to be feasible.

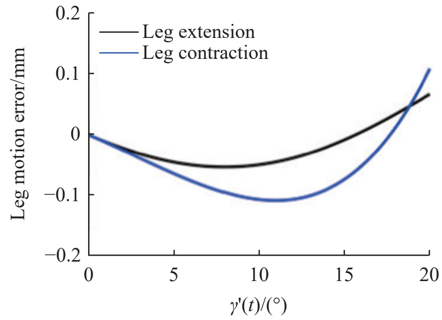

Figure 8 Leg motion error with $\gamma'(t)$

3.1.2 Control part calculation

The PID controller continuously calculates the error value by determining the difference between the target set point and the process variable being tested. It then utilizes a linear combination of proportional, integral, and derivative errors as the control input[39]. The deviation values $e(\theta)$ and $e(d)$ are obtained by subtracting the values $\theta(t)$ and $d(t)$ collected by the corresponding sensors from the calculated values $\theta^*(t)$ and $d^*(t)$, respectively. $e(\theta)$ and $e(d)$ satisfy the follows:

$$\begin{cases} e(\theta) = \theta^*(t) - \theta(t) \\ e(d) = d^*(t) - d(t) \end{cases} \tag{12}$$

In order to reduce the rotation amount of the deflection mechanism and ascertain its rotational orientation, set conditions:

$$\begin{aligned} &\begin{cases} e'(\theta) = e(\theta) \\ e'(d) = e(d) \end{cases}, \ (|e(\theta)| \le 90^\circ) \\ &\begin{cases} e'(\theta) = e(\theta) - 180^\circ \\ e'(d) = -e(d) \end{cases}, \ (90^\circ < e(\theta) \le 270^\circ) \\ &\begin{cases} e'(\theta) = e(\theta) - 360^\circ \\ e'(d) = e(d) \end{cases}, \ (270^\circ < e(\theta) < 360^\circ) \\ &\begin{cases} e'(\theta) = e(\theta) + 180^\circ \\ e'(d) = -e(d) \end{cases}, \ (-270^\circ < e(\theta) \le -90^\circ) \\ &\begin{cases} e'(\theta) = e(\theta) + 360^\circ \\ e'(d) = e(d) \end{cases}, \ (-360^\circ < e(\theta) < -270^\circ) \end{aligned} \tag{13}$$

The $e'(\theta)$ value is in the range of [–90°, 90°], and the $e'(d)$ value is in the range of [15.76, 15.81] mm.

During the leveling process, the time required for the stepper motor to drive the deflection mechanism to rotate should be equivalent to that of the linear motor driving the deflection mechanism to tilt, that is

$$\frac{|e'(\theta)|}{w(t)} = \frac{|e'(d)|}{v(t)} \tag{14}$$

When $e'(\theta)$, $e'(d)$ reach the maximum value $e'_{\max}(\theta)$, $e'_{\max}(d)$, the fastest leveling time t is

$$t = \max\left(\frac{e'_{\max}(\theta)}{w_{\max}}, \frac{e'_{\max}(d)}{v_{\max}}\right) = \frac{e'_{\max}(d)}{v_{\max}} \tag{15}$$

where, $w_{\max}$ is the maximum speed limit for the stepper motor, rad/s; $v_{\max}$ is the maximum speed limit for the linear motor, mm/s. Therefore, the maximum speed $v_{\max}$ of the linear motor is selected as a reference, and the maximum speed $w'_{\max}$ of the actual operation of the stepper motor is controlled. The ratio k of $w'_{\max}$ and $v_{\max}$ can be obtained from Equations (11) and (14).

$$k = \frac{w'_{\max}}{v_{\max}} = \frac{e'_{\max}(\theta)}{e'_{\max}(d)} = \frac{e'_{\max}(\theta)}{k_d \gamma_{\max}} = 5.7 \tag{16}$$

where, $\gamma_{\max}$ is the upper limit leveling angle of the leveling platform, (°); $\gamma_{\max}$=20°.

In order to make the stepper motor and linear motor use the same controller, the control deviation $e(t)$ is first screened to make it satisfy

$$e(t) = \max\left(\frac{|e'(\theta)|}{k}, |e'(d)|\right) \tag{17}$$

The discrete PID control methods can be categorized into positional type and incremental type[40]. In this study, positional PID control algorithm is selected. Due to the existence of leveling threshold, only proportional control (P control) is required to swiftly adjust the platform within the threshold range, and the output result $u_{\theta,d}(t)$ is

$$u_{\theta,d}(t) = K_{\mathrm{P}} e(t) \tag{18}$$

where, K_{P} is the dynamic leveling proportional coefficient. The output result of the controller is restored.

$$\begin{aligned} &\begin{cases} w(t) = k u_{\theta,d}(t) e'(\theta) / |e'(\theta)| \\ v(t) = u_{\theta,d}(t) e'(d) / |e'(\theta)| \end{cases}, \ \left(\frac{|e'(\theta)|}{k} \ge |e'(d)|\right) \\ &\begin{cases} w(t) = k u_{\theta,d}(t) e'(\theta) / (|e'(d)|) \\ v(t) = u_{\theta,d}(t) e'(d) / |e'(d)| \end{cases}, \ \left(\frac{|e'(\theta)|}{k} < |e'(d)|\right) \end{aligned} \tag{19}$$

3.1.3 Output part calculation

When the platform inclination is significant, the coordinated control of the linear motor and stepper motor ensures that if a drive component's speed was faster in the previous cycle, it will be reduced in the subsequent cycle under this coordination. Conversely, if a drive component's speed was slower in the previous cycle, it will be increased in the next cycle. Consequently, changes in linear motor speed have minimal impact on leveling results. Therefore, the speed of the linear motor is controlled directly by adjusting the duty ratio R_D; the duty ratio size is 0-100%, and the duty ratio is satisfied:

$$R_{\mathrm{D}} = \frac{v(t)}{v_{\max}}\left(100\% - R_0\right) + R_0 \tag{20}$$

where, R_0 is the minimum duty ratio for the motor to start under load, and the positive or negative value of R_D represents the direction of movement of the linear motor.

The speed of the stepper motor is controlled by adjusting the pulse frequency[41], and the speed of the stepper motor is satisfied:

$$w(t) = \frac{60 f \tau_0 \tau_1}{\frac{360}{S} X} = \frac{f S \tau_0 \tau_1}{60X} \tag{21}$$

where, f is the pulse frequency that the controller needs to output, Hz; τ_0 is the reduction ratio of the reducer; τ_1 is the tooth ratio of the tooth bearing to the active gear; S is the step angle of the stepper motor, (°); X is the microstepping factor of the stepper motor driver.

According to Equation (21), the pulse frequency that the controller needs to output can be obtained as,

$$f = \frac{60 X w(t)}{T \tau_0 \tau_1} \tag{22}$$

The positive or negative value of f represents the direction of movement of the stepper motor.

3.2 Static control strategy

When the inclination of the platform is below the threshold value, the vertical acceleration output provided by the chassis attitude sensor is utilized to determine whether the chassis is in motion. In cases where the chassis remains stationary, the leveling platform is used for static leveling. The static control strategy analyzes the control of static leveling based on dynamic control strategy. The input part of static control is essentially identical to that of dynamic leveling, but it necessitates higher precision based on static leveling. An accurate calculation value of $d'(t)$ in Equation (10) is adopted to adjust the telescoping distance of the support legs, and the displacement $d^*(t)$ of the linear motor satisfies

$$d^*(t) = d'(t)/3.25 \tag{23}$$

In the control part, an integral link (PI control) is introduced to reduce the steady-state error[42]. Because the inclination is small, it is unnecessary to coordinate the speed of the stepper motor and the linear motor at this time. According to Equation (13), $w(t)$ and $v(t)$ can be expressed as,

$$\begin{cases} w(t) = K_{\mathrm{P}\theta} e'(\theta) + \sum K_{\mathrm{I}\theta} e'(\theta) \\ v(t) = K_{\mathrm{P}d} e'(d) + \sum K_{\mathrm{I}d} e'(d) \end{cases} \tag{24}$$

where, $K_{\mathrm{P}\theta}$, $K_{\mathrm{I}\theta}$ are the proportional coefficient and integral coefficient of the stepper motor in the static leveling process, respectively. K_{Pd}, K_{Id} are the proportional coefficient and integral coefficient of the linear motor in the static leveling process respectively.

4 Control system simulation analysis

4.1 Control parameter analysis

In order to evaluate P and I control parameters in each stage of the controller, Matlab/Simulink was developed to establish the leveling simulation model of the static state of the chassis, as shown in Figure 9. Where $\theta^*(t)$ and $\gamma'(t)$ are input signals, while the integral of the deflection mechanism rotation signifies data measured by the hall angle sensor, the integral of linear motor movement represents data measured by the displacement sensor. The difference between $\gamma'(t)$ before and after the movement indicates platform slope, with vertical acceleration of the chassis set to 0.

The simulation employed a two-factor and two-level full-factor experiment to debug the control parameters. The low level of $\gamma'(t)$ was set at a leveling threshold of 2°, while the high level corresponded to a limit deflection angle of 20°. For the low level of $\theta^*(t)$ takes 9° through Equation (17), while the high level takes the limit angle of 90°. Resulting from the cross combination ($\gamma'(t)$, $\theta^*(t)$), respectively, (2°, 9°), (2°, 90°), (20°, 9°), and (20°, 90°). The starting duty ratio R_0 of the linear motor is 10%, and the maximum speed v_{max} is 10.5 mm/s. The stepper motor's maximum speed w'_{max} in the dynamic leveling stage is 117 r/min, while in the static leveling stage, it reaches 175 r/min. After debugging, the dynamic leveling parameter is determined as K_P=7, and the static leveling parameters are determined as $K_{P\theta}$=10.5, $K_{I\theta}$=0.1, K_{Pd}=5, K_{Id}=0.4. The simulation results under these parameters are shown in Figure 10. From Figures 10a and 10b, the response curves of $\gamma'(t)$ and $\theta^*(t)$ in the static leveling stage demonstrate that the target position can be rapidly achieved by independently controlling the linear motor and stepper motor. Moreover, these curves exhibit minimal overshoot and steady-state error. From Figures 10c and 10d, the coordinated control of the linear motor and stepper motor enables $\gamma'(t)$ and $\theta^*(t)$ to rapidly and accurately reach the target position during the dynamic leveling stage. The simulation results demonstrate the control system's excellent adaptability.

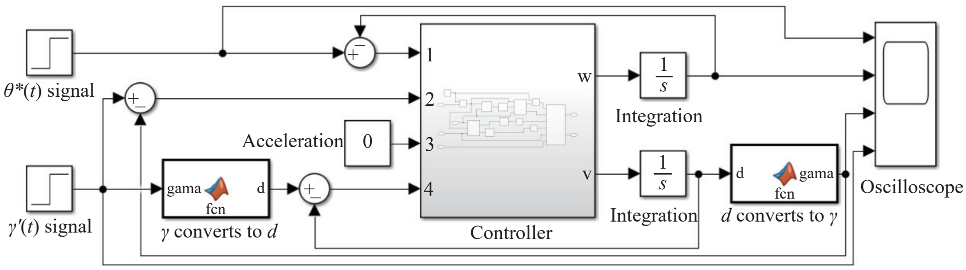

Figure 9 Chassis static state simulation model

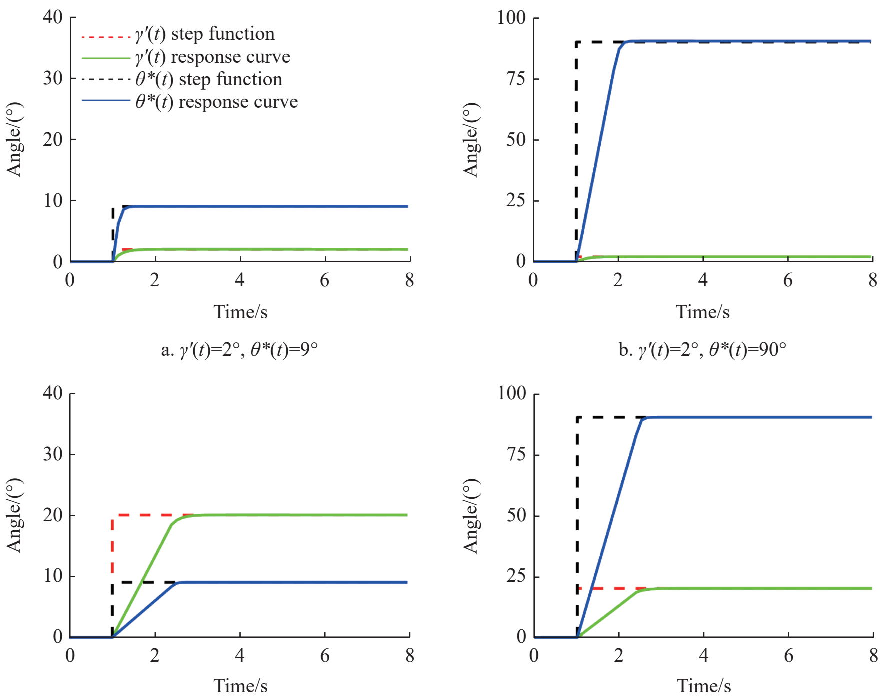

a. $\gamma'(t)$=2°, $\theta^*(t)$=9°
b. $\gamma'(t)$=2°, $\theta^*(t)$=90°
c. $\gamma'(t)$=20°, $\theta^*(t)$=9°
d. $\gamma'(t)$=20°, $\theta^*(t)$=90°

Figure 10 Simulation results of chassis static state

4.2 Recurdyn-Simulink co-simulation

In order to evaluate the overall performance of the control system, the 3D model of the crawler chassis is initially established in Recurdyn software. Subsequently, the leveling platform designed using SolidWorks is simplified and imported into Recurdyn for assembly. The simulation incorporates appropriate materials for each component and establishes connection pairs between them (see Table 1). The connecting pairs of the base and the lower rotary table, as well as the push rod and the push rod housing, are driven respectively by a rotating motor and a linear motor. Figure 11 shows the established kinematics simulation model. In the model, the overall size of the leveling platform is 0.475 m×0.450 m×0.600

m (L×W×H), and the height between the base and the platform is 0.365 m. The overall size of the track chassis is 0.868 m×0.680 m×0.300 m (L×W×H), the track width is 0.100 m, the track grounding length is 0.467 m, and the ground slope is 15°.

Table 1 Connection relationship of each part in the system

Connecting part	Connecting pair
Base and chassis	Fixed
Base and telescoping mechanism	Spherical
Base and upper rotary table	Revolute
Lower rotary table and supporting leg	Revolute
Lower rotary table and adjusting legs	Revolute
Platform and upper rotary table	Revolute
Platform and telescoping mechanism	Revolute
Inside of telescoping mechanism	Cylindrical
Push rod and push rod housing	Cylindrical

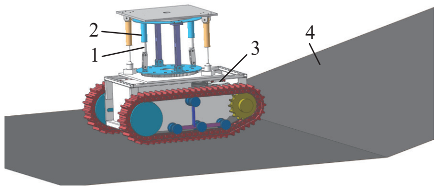

1. Push rod; 2. Push rod housing; 3. Track chassis; 4. Ground

Figure 11 Simulation kinematics model of leveling platform

The input and output parameters of the model should be configured in the Communicator module within Recurdyn. Specifically, the output parameters of Recurdyn serve as input functions for Simulink, while the input parameters of Recurdyn correspond to the output functions of Simulink. During the simulation process, Simulink is utilized as the primary program for executing the simulation. After setting the chassis to drive from the flat ground to the slope, it turned 180° on the slope and drove off the slope to the flat ground. The pitch angle and roll angle changes of the platform and the chassis were recorded. The co-simulation model is shown in Figure 12.

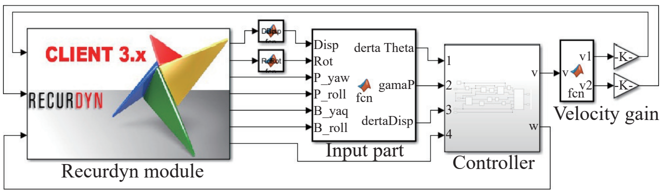

Figure 12 Recurdyn-Simulink co-simulation model

Considering that the working speed of the tea plantation machinery is about 0.5 m/s[43,44], the forward speed of the chassis is set to be 0.3 m/s, 0.5 m/s, and 0.7 m/s respectively in the simulation, and the simulation results are shown in Figure 13. Figure 13 demonstrates that the platform achieves a fundamental level of stability across various vehicle speeds. However, as the traveling speed increases, the rate at which the chassis inclination changes accelerates, the time required for leveling is shortened, and the leveling effect becomes worse. During the ascending and descending slope phases, significant changes in pitch angle and platform inclination occur, leading to a potential impact on the stability of leveling performance due to excessive travel speed. Specifically, when the travel speed increases from 0.3 to 0.7 m/s, the pitch angle, roll angle, and platform inclination increase from 1.56°, 0.81°, and 1.56° to 6.10°, 1.06°, and 6.10°, respectively. During the turning process, the changes in pitch angle, roll angle, and platform inclination are significantly smaller compared to those during the ascending and descending slope phases, remaining within the platform's slope threshold. The simulation results validate the rationality of the leveling control strategy, demonstrating that the platform can achieve omnidirectional dynamic leveling. Moreover, a more effective leveling effect can be attained by reducing chassis speed in areas with abrupt changes in slope.

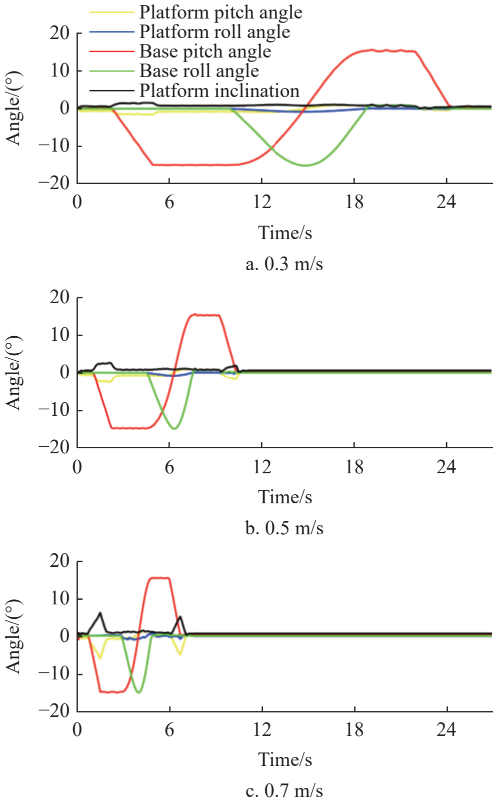

Figure 13 Results of co-simulation at different forward speed of the chassis

5 Performance test

5.1 Preparation and evaluation index in field test

In this study, the leveling control system was installed on the designed leveling platform, which was mounted on a small self-propelled track chassis for prototype testing. The laboratory prototype test is shown in Figure 14. The overall size of the leveling system prototype is 0.868 m×0.680 m×0.600 m (L×W×H), the track width is 0.100 m, and the track grounding length is 0.467 m. A computer is used as the upper computer to receive real-time pitch angle and roll angle data of the chassis and platform.

Figure 14 Laboratory prototype test

The evaluation parameters of static leveling performance in this paper are platform inclination adjustment error γ_e and leveling time T_{adj}, shown in Equations (25) and (26). The evaluation parameters of field dynamic leveling performance are selected as platform inclination mean $\bar{\gamma}$ and platform standard deviation S_γ, shown in Equations (27) and (28)[45].

$$\gamma_e = \frac{1}{20}\sum_{i=i_e}^{i_e+19}\gamma_i \tag{25}$$

$$T_{\text{adj}} = T(i_e - i_s) \tag{26}$$

$$\bar{\gamma} = \frac{1}{N}\sum_{i=1}^{N}\gamma_i \tag{27}$$

$$S_\gamma = \sqrt{\frac{1}{N-1}\sum_{i=1}^{N}\left(\gamma_i - \bar{\gamma}\right)^2} \tag{28}$$

where, γ_i is the inclination corresponding to the sampling point, (°); T is the sampling period of the system, s; i_s is the number of sampling points of the pitch angle and roll angle recorded at the beginning of system adjustment; i_e is the number of sampling points of the pitch angle and roll angle recorded at the completion of system adjustment; N is the total number of data points recorded in a single test.

5.2 Response speed test

To evaluate the system response time, a test is conducted under small inclination angles and low vehicle speeds so that the response curve could be clearly observed. When the platform attitude information indicates that leveling is required, the microcontroller outputs a high-level signal. Once the platform starts the leveling motion, this high-level signal is pulled low. A logic analyzer was used to monitor the high/low-level output of the microcontroller. As shown in Figure 15, the recorded high/low-level response and the time histories of the inclination angles of the platform and the base collected during the test are presented. The two sets of results corroborate each other, confirming the accuracy of the measurements. The measured system response time was 0.121 s, which is sufficient to meet the requirements of dynamic leveling of the platform. This demonstrates that the leveling system can efficiently regulate the platform pitch and roll angles, thereby maintaining the platform in a relatively stable balanced state.

5.3 Static leveling performance test

The adjustment range commonly used in the mountain tea plantation environment is 0°-15°. In this study, a static leveling test of the leveling system was conducted on a 15° slope using the comprehensive performance test platform for "soil-mechanical-crop" in the hilly and mountainous areas of Northwest A&F University in March 2024, as shown in Figure 14. During the test, the chassis started the leveling function on the flat ground to achieve platform stability, turned off the leveling function, then the chassis ascended a 15° slope, and adjusted the angle of the chassis to eight initial states: lowest front, lowest back, lowest left, lowest right, lowest front left, lowest front right, lowest back left, and lowest back right. The combination (α_0, β_0) of pitch angle α_0 and roll angle β_0 for the eight initial states of chassis is shown in Figure 16. The leveling function was then activated, and the changes in the pitch and roll angles of the platform over time were recorded. The test results are shown in Figure 17, with the initial leveling time being 1.9 s.

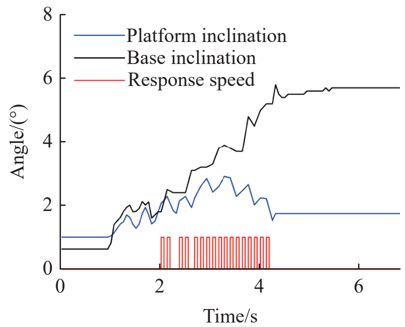

Figure 15 Results of response speed test

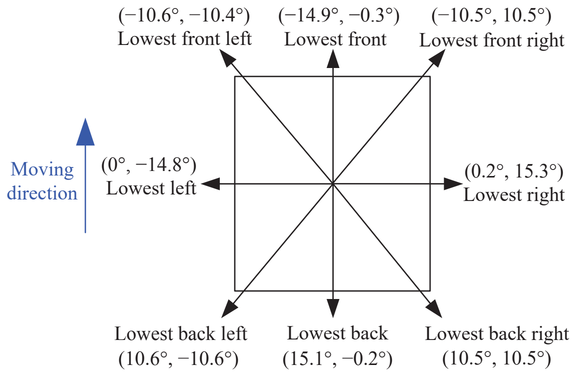

Figure 16 Chassis initial state diagram

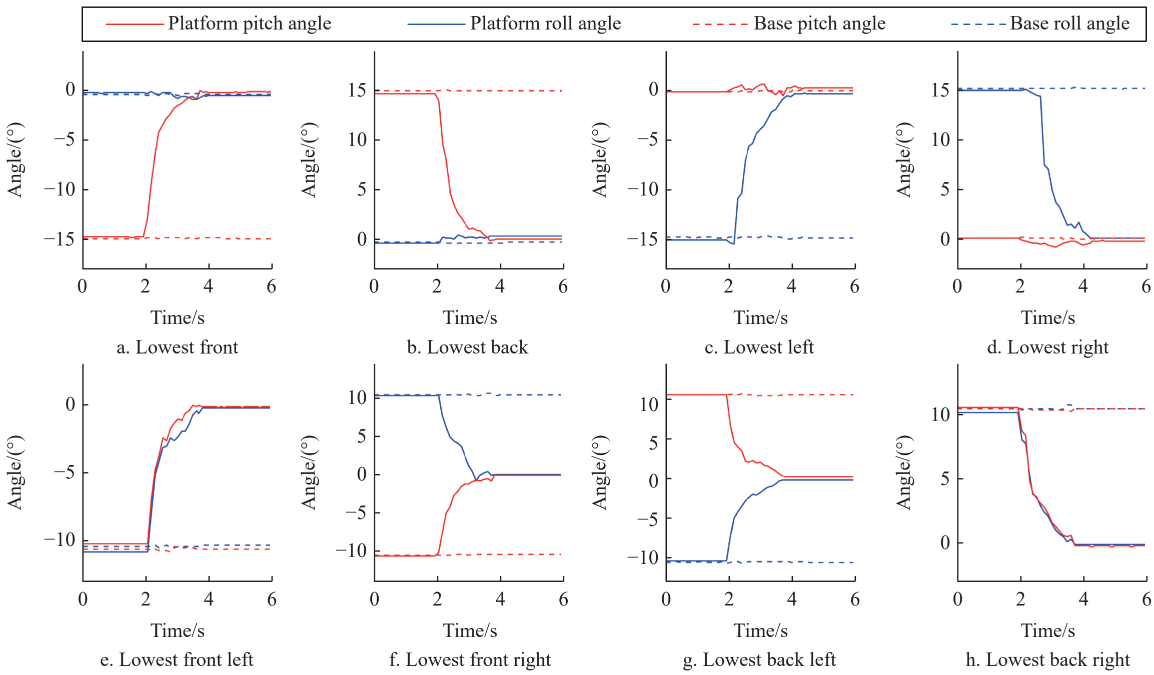

a. Lowest front b. Lowest back c. Lowest left d. Lowest right

e. Lowest front left f. Lowest front right g. Lowest back left h. Lowest back right

Figure 17 Static leveling test results

As can be seen from Figure 17, the chassis undergoes adjustments from eight different initial inclination states, with the platform's initial inclinations being 14.7°, 14.8°, 15.0°, 15.1°, 14.8°, 14.8°, 14.8°, and 14.7° respectively. Due to the presence of threshold values, the adjustment durations are as follows: 1.9 s, 1.8 s, 2.3 s, 2.3 s, 1.9 s, 1.9 s, 1.8 s, 1.8 s. The adjustment errors of the inclination are 0.4°, 0.4°, 0.4°, 0.2°, 0.2°, 0.1°, 0.3°, 0.2°, respectively. The shortest leveling time was 1.8 s, the longest was 2.3 s, and the average adjusting time was 2.0 s. The maximum inclination adjustment error is 0.4°, the minimum is 0.1°, and the average is 0.3°, which conforms to the static leveling threshold parameter. Comparing the eight adjustment processes, the leveling time of the platform is longest when the initial state of the lowest left and lowest right is utilized. The reason is that during the test, it was observed that when the deflection mechanism's angle of rotation $|e'(\theta)|$ falls within the range of 45°-90°, significant changes in the pitch angle of the platform occur due to any action of the linear motor if no coordinated control restrictions are imposed on both the linear motor and stepper motor. The restriction condition added to the coordinated control of the linear motor and the stepper motor in order to address this issue is as follows: when $|e'(\theta)|$ falls within the range of 45°-90°, there will be no movement from the linear motor. The platform is capable of descending to below 5° within 1 s at an inclination of 15°, demonstrating the leveling system's ability to rapidly and comprehensively level at a significant incline, effectively validating the efficiency and precision of the designed control system.

5.4 Field performance test

The platform is susceptible to significant changes in pitch angle and roll angle when entering or exiting the tea plantation. In order to verify the dynamic leveling performance of the entire machine, a field test was conducted in April 2024 at the Xixiang Tea Experimental Demonstration Station of Northwest A&F University. To meet the actual operating conditions of the platform, tea plantation operating equipment needs to be installed on the leveling platform. The operating equipment carried in this article is a tea-picking machine, and the chassis is controlled to drive into and out of the tea plantation, as shown in Figure 18. The tea-picking machine mounted on the platform was modified from an SV120 two-person tea harvester. The original machine weighed 16 kg. After modification, a lifting mechanism was added to accommodate tea plants of different heights, and the gasoline engine was replaced with an electric motor to meet environmental requirements. The total mass of the modified machine is 49 kg, which is lower than the platform's designed rated payload of 60 kg. The testing distance is set as 5 m. During the test, the leveling function is activated, and remote control is used to drive the chassis into and out of the tea plantation. The pitch angle and roll angle of both the platform and the base are recorded, with the test results shown in Figure 19.

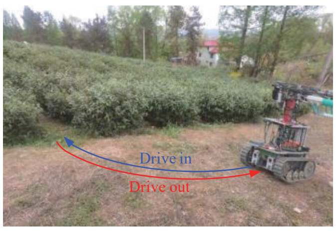

Figure 18 Tea plantation field test

As can be seen from Figure 19, the pitch angle and roll angle of the platform compared to the ground were significantly improved in the field test. In the process of driving into and out of the tea plantation, the mean values of the inclination of the chassis were 11.8° and 11.9° with the standard deviations of 3.1° and 3.3°, respectively, indicating that the terrain was inclined and had a large undulation. In the process of the chassis driving into the tea plantation, the platform inclination ranges from 0.5° to 6.3°, with a mean value of 3.2° and the standard deviation value of 1.5°. In the process of the chassis driving out of the tea plantation, the platform inclination ranges from 0.5° to 6.5°, with the mean value of 2.5° and the standard deviation value of 1.4°. The results show that the proposed leveling control system enables rapid platform leveling, mitigating the risk of overturning caused by lateral inclination of the entire machine during operations in hilly and mountainous tea plantations, thereby enhancing overall operational efficiency in such terrains. Compared with the dynamic leveling systems reported in References [22,45], the leveling system proposed in this study features a wider leveling-angle range, which leads to a longer leveling time under large-inclination conditions. To shorten the leveling time, only P control was adopted for both the linear motor and the stepper motor, which inevitably introduces a steady-state error. Nevertheless, the dynamic leveling accuracy remains within an acceptable range for engineering applications. Compared with the static leveling systems presented in References [46,47], the proposed system exhibits a slight reduction in leveling accuracy. This is mainly attributable to the limited measurement accuracy of the attitude sensor: if the static leveling threshold is set too small, the system tends to enter repeated leveling cycles, thereby impairing normal platform operation. The static leveling accuracy could be further improved by replacing the attitude sensor with a higher-precision one.

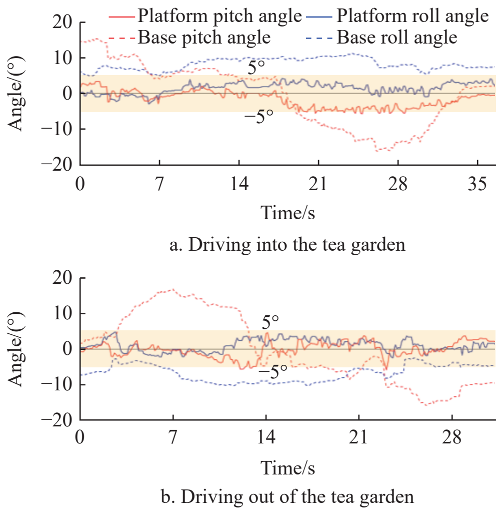

a. Driving into the tea garden

b. Driving out of the tea garden

Figure 19 Results of field test

6 Conclusions

This study proposed a dynamic and static joint leveling control system based on PID, providing a novel technical solution for the development of self-propelled tea canopy working machines suitable for mountainous tea plantations. In order to meet the requirements of different working conditions in tea plantation operation, a static leveling strategy was developed based on dynamic leveling. Numerical simulations and field tests demonstrate the following major conclusions:

Firstly, the control system coordinates the linear motor and stepper motor to achieve dynamic leveling, while static leveling further suppresses overshoot and steady-state error, improving system adaptability. Secondly, the dynamic and static joint leveling control strategy is developed and its parameters (dynamic K_P=7; static $K_{P\theta}$=10.5, $K_{I\theta}$=0.1, K_{Pd}=5, K_{Id}=0.4) are identified via static chassis-leveling simulations and validated through Recurdyn-Simulink co-simulation. Finally, tests show that under 15.0° static leveling, the inclination error is 0.1°-0.4° with a leveling time of 1.8-2.3 s, and the inclination reduces to below 5.0° within 1.0 s. As the results of field tests, the mean platform inclinations of 3.2°±1.5° and 2.5°±1.4° when entering and leaving the tea plantation, demonstrating stable operation and confirming omnidirectional dynamic leveling capability.

Although our self-developed vehicle leveling platform was designed to solve the problem of tea plantation operations, it is clear that it can also be used for the operation of other mountain crops. In our future work, two limitations on the current model will be addressed. One is that the present system is a passive leveling system, and the quality of leveling can only be improved by reducing driving speed. The other is that the slope threshold for the leveling control system is too large, indicating that the accuracy of leveling needs to be improved.

Acknowledgements

This study was supported by the Shaanxi Province Key Research and Development Plan project (Grant No. 2024NC-YBXM-205) and China Agriculture Research System of MOF and MARA (Grant No. CARS-19).

[References]

[1] Ahammed G, Li X. Hormonal regulation of health-promoting compounds in tea (*Camellia sinensis* L). Plant Physiology and Biochemistry, 2022; 185: 390–400.

[2] Du Z, Li D, Ji J, Zhang L, Li X, Wang H. Bionic optimization design and experiment of reciprocating cutting system on single-row tea harvester. Agronomy, 2022; 12: 1309.

[3] Wu Y, Chen J, Wu S, Li H, He L, Zhao R, et al. An improved YOLOv7 network using RGB-D multi-modal feature fusion for tea shoots detection. Computers and Electronics in Agriculture, 2024; 216: 108541.

[4] Qin K, Liang X, Cao C, Ding W, Wu Z, Fang L. Design and experiment of combined cutting and throwing sitching blade for tea plantation. Transactions of the Chinese Society for Agricultural Machinery, 2021; 52(5): 74–82.

[5] Liu A, Wu J, Zhang F, Yang W, Wang H, Gang X. Studies on a statically determinate leveling control strategy for a statically indeterminate four-leg support vehicle-borne platform. Mechanics Based Design of Structures and Machines, 2023; 51(12): 7131–7148.

[6] Dorling C M, Zinober A S I. Hyperlane design in model-following variable structure control systems. IFAC Proceedings Volumes, 1985; 18(5): 1901–1905.

[7] Hays G G, Pearson K L. Multirole survivable radar-balancing threats and technology. Proceedings of the IEEE National Radar Conference, Dallas: IEEE, 1989; pp.13-19. doi: 10.1109/NRC.1989.47608.

[8] Xiao J, Wang Y, Li X, Zheng J. Design of high precision mechatronic-hydraulic leveling system for vehicle-mounted radar. Journal of Physics: Conference Series, 2021; 2113(1): 012041.

[9] Tihonov A, Velichkin V. Paver automation for road surfacing. Conference Series: Earth and Environmental Science, 2017; 90: 012148.

[10] Teng R M, Wang X, Wang J Z, Liang J F. Research on vibration suppression for boom luffing of telescopic boom aerial work platform. In: Intelligent Computing and Internet of Things. ICSEE IMIOT 2018. Springer Singapore, 2018; 924: 330–341.

[11] Zhao J, Ma H F, Zhao Z R. The application of parametric method in the stability analysis of aerial work platform. Journal of Physics: Conference Series, 2022; 2170(1): 012002.

[12] Nie Z, Wang H, Lu B, Zhang F, Wang M, Wu Z, et al. Development and first test of an attitude and load coupling adjustment chassis for aerial working platforms. Mechanics Based Design of Structures and Machines, 2024; 52(4): 2066–2084.

[13] Sun J, Meng C, Zhang Y, Chu G, Zhang Y, Yang F, et al. Design and physical model experiment of an attitude adjustment device for a crawler tractor in hilly and mountainous regions. Information Processing in Agriculture, 2020; 7(3): 466–478.

[14] Yang F, Niu H, Sun J, Liu Z, Li Y, Chu H. Design and experiment of attitude cooperative control system of mountain crawler tractor and farm tools. Transactions of the Chinese Society for Agricultural Machinery, 2022; 53(1): 414–422. (in Chinese)

[15] Denis D, Thuilot B, Lenain R. Online adaptive observer for rollover avoidance of reconfigurable agricultural vehicles. Computers and Electronics in Agriculture, 2016; 126: 32–43.

[16] İrsel G, Altinbalik M T. Adaptation of tilt adjustment and tracking force automation system on a laser-controlled land leveling machine. Computers and Electronics in Agriculture, 2018; 150: 374–386.

[17] Wang Z, Ma W, Wang T, Liu C. Body leveling control model establishment and experiment analysis. Applied Engineering in Agriculture, 2022; 38(2): 243–251.

[18] Hu J, Pan J, Dai B, Chai X, Sun Y, Xu L. Development of an attitude adjustment crawler chassis for combine harvester and experiment of adaptive leveling system. Agronomy, 2022; 12(3): 717.

[19] Federico D, Matteo C, Daniele D'A, Andrea A, Francesco T, Matteo S S. Modeling, control design and experimental automatic calibration of a leveling system for combine harvesters. Control Engineering Practice, 2023; 132: 105411.

[20] Park Y, Son H I. A sensor fusion-based cutting device attitude control to improve the accuracy of Korean cabbage harvesting. Journal of the ASABE, 2022; 65(6): 1387–1396.

[21] Park Y, Kim H J, Son H I. Novel attitude control of Korean cabbage harvester using backstepping control. Precision Agriculture, 2023; 24: 744–763.

[22] Wang Z, Yang J, Liu P, Long X, Li H, Wei W. Development of an agricultural vehicle levelling system based on rapid active levelling. Biosystems Engineering, 2019; 186: 337–348.

[23] Acuña-Bravo W, Canuto E, Agostani M, Bonadei M. Proportional electrohydraulic valves: an embedded model control solution. Control Engineering Practice, 2017; 62: 22–35.

[24] Zhao R, Li X, Chen J. Eagle-inspired manipulator with adaptive grasping and collapsible mechanism and modular DOF for UAV operations. Computers and Electronics in Agriculture, 2023; 215: 108344.

[25] Guzmán J L, Hägglund T. Tuning rules for feedforward control from measurable disturbances combined with PID control: a review. International Journal of Control, 2024; 97(1): 2–15.

[26] Jiang Y, Sun Z, Wang R, Ding R, Ye Q. Design and control of a new omnidirectional levelling system for hilly crawler work machines. Computers and Electronics in Agriculture, 2024; 218: 108661.

[27] Chen W, Hu L, Wang G, Yuan J, Bao G, Shen H, et al. Design of 4UM-120D electric leafy vegetable harvester cutter height off the ground automatic control system based on incremental PID. Agriculture, 2023; 13(4): 905.

[28] Li J, Wang S, Zhang W, Li H, Zeng Y, Wang T, et al. Research on path tracking for an orchard mowing robot based on cascaded model predictive control and anti-slip drive control. Agronomy, 2023; 13(5): 1395.

[29] Yang R, Chen D, Zha X, Pan Z, Shang S. Optimization design and experiment of ear-picking and threshing devices of corn plot kernel harvester. Agriculture, 2021; 11(9): 904.

[30] Wang H, Liu Y, Zhou L, Zhou H, Niu K, Xu M. Design and test of fertilizer flow piecewise PID control system of fertilizer planter. Transactions of the Chinese Society for Agricultural Machinery, 2023; 54(2): 32–40. (in Chinese)

[31] Liang J, Pan F, Chen J, Zhang H, Ji C. A precise simultaneous sowed control system for maize seed and fertilizer. Agriculture, 2024; 14(2): 192.

[32] Mozhdeh M, Payam Z, Mohammad D, Kourosh V, Hamed E. Design and analysis of an aerial pollination system for walnut trees. Biosystems Engineering, 2022; 225: 83–98.

[33] Karadol H, Aybek A, Ucgul M, Kuzu H, Gunes M. Field sprayer with application rate control using fast response proportional valves under variable speed conditions. Agriculture, 2024; 14: 361.

[34] Wu W, Zhang Z, Zhang X, He Y, Fang H. Application of visual inertia fusion technology in rice transplanter operation. Computers and Electronics in Agriculture, 2024; 221: 108990.

[35] Hammoodi S J, Flayyih K S, Hamad A R. Design and implementation

speed control system of DC motor based on PID control and matlab simulink. International Journal of Power Electronics and Drive Systems, 2020; 11(1): 127–134.
[36] Raikwar S, Fehrmann J, Herlitzius T. Navigation and control development for a four-wheel-steered mobile orchard robot using model-based design. Computers and Electronics in Agriculture, 2022; 202: 107410.
[37] Visioli A. PID control system design and automatic tuning using MATLAB/SIMULINK. IEEE Control Systems Magazine, 2021; 41(3): 99–100.
[38] Guo H, Lu H, Gao G, Wu T, Chen H, Qiu Z. Design and test of a levelling system for a mobile safflower picking platform. Applied Sciences, 2023; 13(7): 4465.
[39] Wei X, Huang S. Intelligent laser leveling control system for cement concrete based on MCU control. Journal of Physics: Conference Series, 2021; 1885: 042041.
[40] Zhu Q, Wu G, Zhu Z, Zhang H, Gao Y, Chen L. Design and test on winter wheat precision separated layer fertilization and wide-boundary sowing combined machine. Transactions of the Chinese Society for Agricultural Machinery, 2022; 53(2): 25–35. (in Chinese)
[41] Deng C, Bian E, Ge Z. Design and realization of stepping motor drive system controlled by single-chip microcomputer. Wireless Personal Communications, 2022; 124(4): 1–22.
[42] Ruan C, Zhao D, Sun Y, Hong J, Ding S, Luo J. Design and testing of a control system associated with the automatic feeding boat for farming Chinese river crabs. Computers and Electronics in Agriculture, 2018; 150: 14–25.
[43] Cheng F, Yi W, Tuo H, Wang P, Qiu Y. Design and experiment of tracked self-propelled tea tree top trimmer. Forum of South China, 2020; 51(07): 6–8. (in Chinese)
[44] Du X, Hong F, Ma Z, Zhao L, Zhuang Q, Jia J, et al. CYVIO: A visual inertial odometry to acquire real-time motion information of profiling tea harvester along the planting ridge. Computers and Electronics in Agriculture, 2024; 224: 109116.
[45] Jin C, Yang T, Liu G, Wang T, Chen M, Liu Z. Design and experiment of crawler combine omnidirectional leveling chassis. Transactions of the Chinese Society for Agricultural Machinery, 2020; 51(11): 393–402. (in Chinese)
[46] Chen R, Ou Y, Fang W, Shi Y, Liu L. Simulation analysis of a self-balancing hydraulic platform for agricultural machinery in mountainous regions. Journal Européen des Systèmes Automatisés, 2020; 53(2): 203–211.
[47] Cao P, Wang T, Zhai L, Niu S, Liu L, Shi Y. Design of 6-DOF tomato picking lifting platform. Agriculture, 2022; 12(11): 1945.